

Quark matter nucleation in neutron stars and astrophysical implications

Ignazio Bombaci^{1,2,3}, Domenico Logoteta², Isaac Vidaña⁴ and Constança Providência⁴

¹ Dipartimento di Fisica “E. Fermi”, Università di Pisa, Largo B. Pontecorvo, 3, I-56127 Pisa, Italy

² INFN, Sezione di Pisa, Largo B. Pontecorvo, 3, I-56127 Pisa, Italy

³ European Gravitational Observatory, Via E. Amaldi, I-56021 S. Stefano a Macerata, Cascina Italy

⁴ CFisUC, Department of Physics, University of Coimbra, PT-3004-516 Coimbra, Portugal

Received: date / Revised version: date

Abstract. A phase of strong interacting matter with deconfined quarks is expected in the core of massive neutron stars. We investigate the quark deconfinement phase transition in cold ($T = 0$) and hot β -stable hadronic matter. Assuming a first order phase transition, we calculate and compare the nucleation rate and the nucleation time due to quantum and thermal nucleation mechanisms. We show that above a threshold value of the central pressure a pure hadronic star (HS) (*i.e.* a compact star with no fraction of deconfined quark matter) is metastable to the conversion to a quark star (QS) (*i.e.* a hybrid star or a strange star). This process liberates an enormous amount of energy, of the order of 10^{53} erg, which causes a powerful neutrino burst, likely accompanied by intense gravitational waves emission, and possibly by a second delayed (with respect to the supernova explosion forming the HS) explosion which could be the energy source of a powerful gamma-ray burst (GRB). This stellar conversion process populates the QS branch of compact stars, thus one has in the Universe two coexisting families of compact stars: pure hadronic stars and quark stars. We introduce the concept of critical mass M_{cr} for cold HSs and proto-hadronic stars (PHSs), and the concept of limiting conversion temperature for PHSs. We show that PHSs with a mass $M < M_{cr}$ could survive the early stages of their evolution without decaying to Qs. Finally, we discuss the possible evolutionary paths of proto-hadronic stars.

PACS. 97.60.Jd Neutron stars – 25.75.Nq Quark deconfinement, quark-gluon plasma production, and phase transitions – 26.60.Kp Equations of state of neutron-star matter – 98.38.Mz Supernova remnants – 98.70.Rz γ -ray bursts – 64.60.Qb Nucleation

1 Introduction

Neutron stars, the compact remnants of core-collapse supernova, are the densest macroscopic objects in the Universe. They represent the limit beyond which gravity overwhelms all the other forces of nature and lead to the formation of a black hole. In fact, neutron star structure calculations (see *e.g.* Refs. [1,2,3]) based on a large variety of modern equations of state (EOS) of hadronic matter, predict a maximum stellar central density (the one for the maximum mass star configuration) in the range of 4 – 8 times the saturation density ($\sim 2.8 \times 10^{14}$ g/cm³) of nuclear matter. Thus the core of a neutron star is one of the best candidates in the Universe where a phase of strong interacting matter with deconfined quarks could be found, and these compact stars can be viewed as natural laboratories to test the low temperature T and high baryon chemical potential μ region of the QCD phase diagram.

Current high precision numerical calculations of QCD on a space-time lattice at zero baryon chemical potential (zero baryon density) have shown that at high temperature and for physical values of the quark masses, the transition to quark gluon plasma is a crossover [4,5,6] rather than a real phase transition.

Unfortunately, present lattice QCD calculations at finite baryon chemical potential are plagued with the so called “sign problem”, which makes them unrealizable by all presently known lattice methods. Thus, to explore the QCD phase diagram at low T and high μ , it is necessary to invoke some approximations in QCD or to apply a QCD effective model [7,8,9,10,11,12,13,14,15,16]. In this region of the T - μ plane, several QCD inspired models suggest the deconfinement transition to be a first-order phase transition [17,18]. In this domain of the QCD phase diagram, many possible color superconducting phases of quark matter are expected [19,20] and matter might be characterized by the formation of different crystalline structures [21,22]. It is worth mentioning that recent promising attempts to describe the whole QCD phase diagram within a unified

model [23,24,25,26] (see also [27]) provides a powerful tool to link numerical lattice QCD calculations with measured neutron star masses [28,29,30].

Here, we have adopted a more traditional and simple view, assuming a single first-order phase transition between the confined (hadronic) and deconfined phase of dense matter, and we used rather common models for describing them.

As it is well known, all first order phase transitions are triggered by the nucleation of a critical size drop of the new (stable) phase in a metastable mother phase. This is a very common phenomenon in nature (e.g. fog or dew formation in supersaturated vapor, ice formation in supercooled water) and plays an important role in many scientific disciplines (e.g. atmospheric science, meteorology, cosmology, biology) as well as in many technical applications (e.g. metallurgy).

In the last few years, we have investigated [31,32,33,34,35,36,37,38,39,40,41,42,43,44] (see also Refs. [45,46,47,48,49,50,51,52]) the astrophysical consequences of the nucleation process of quark matter (QM) in the core of massive pure hadronic compact stars (hadronic stars, HSs) *i.e.* neutron stars in which no fraction of QM is present. In this contribution, we report some of the main findings of these studies.

2 Equation of state of dense matter

All the results we report in the present paper are relative to the zero and finite temperature version of the following models for the EOS of dense matter. For the hadronic phase we use the Glendenning–Moszkowski model [53,54], and particularly the GM1 and the GM3 parametrizations [53,54,38]. The nucleon coupling constants are fitted to the bulk properties of nuclear matter. The inclusion of hyperons involves new couplings, which can be written in terms of the nucleonic ones as: $g_{\sigma Y} = x_{\sigma} g_{\sigma}$, $g_{\omega Y} = x_{\omega} g_{\omega}$, $g_{\rho Y} = x_{\rho} g_{\rho}$. In this model [53,54] it is assumed that all the hyperons in the baryonic octet have the same coupling and, in addition, it is assumed that $x_{\rho} = x_{\sigma}$. The binding energy of the Λ particle in symmetric nuclear matter $B_{\Lambda}/A = -28 \text{ MeV} = x_{\omega} g_{\omega} \omega_0 - x_{\sigma} g_{\sigma} \sigma$ is used [53,54] to determine x_{ω} in terms of x_{σ} . In this work we will consider the cases $x_{\sigma} = 0.6$ (hereafter GM1_{0.6}) $x_{\sigma} = 0.7$ (GM1_{0.7}), and $x_{\sigma} = 0.8$ (GM1_{0.8}). Notice that the case with $x_{\sigma} = 0.6$ produces stars with a larger hyperon population (for a given stellar gravitational mass) with respect to the case $x_{\sigma} = 0.7$ and $x_{\sigma} = 0.8$ [54,38].

For the deconfined quark phase we have used the following models: (i) the MIT bag model EOS [55] with $m_s = 150 \text{ MeV}$, $m_u = m_d = 0$, $\alpha_s = 0$ and different values for the bag constant B ; (ii) an extended version of the MIT bag model EOS which includes perturbative corrections due to quark interactions, up to the second order ($\mathcal{O}(\alpha_s^2)$) in the strong structure constant α_s [56,57,58]. This EOS model is parametrized in term of an effective bag constant (B_{eff}) and a perturbative QCD correction term (a_4), whose value represents the degree of deviations from an ideal relativistic Fermi gas EOS, with the case

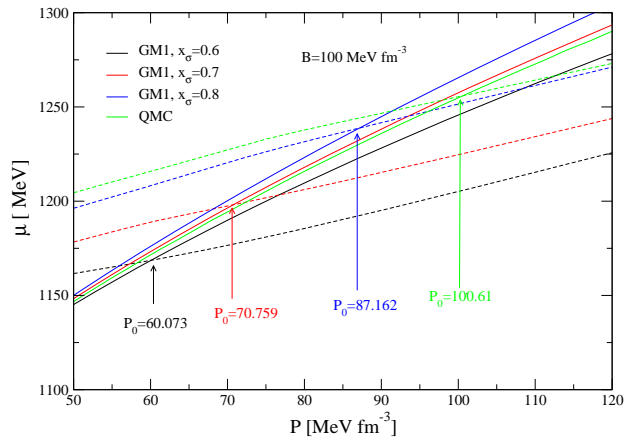


Fig. 1. (Color on line) The Gibbs energy per particle for the β -stable hadronic phase (continuous curves) and for the respective Q^* phase (dashed curves) at $T = 0$. The GM1 and the QMC models have been used for the hadronic phase EOS, and bag model EOS with $B = 100 \text{ MeV}/\text{fm}^3$ for the Q^* -phase.

$a_4 = 1$ corresponding to the ideal gas [56,57,58]. Within this extended bag model one can thus evaluate the non-ideal behaviour of the EOS of cold SQM at high density; (iii) the Nambu–Jona-Lasinio (NJL) model [7], with the lagrangian density given in Ref. [59]; (iv) the Chromo Di-electric model [60,61].

3 Phase equilibrium

For a first-order phase transition the conditions for phase equilibrium are given by the Gibbs’ phase rule

$$T_H = T_Q \equiv T, \quad P_H = P_Q \equiv P_0, \quad \mu_H(T, P_0) = \mu_Q(T, P_0) \quad (1)$$

where

$$\mu_H = \frac{\varepsilon_H + P_H - s_H T}{n_H}, \quad \mu_Q = \frac{\varepsilon_Q + P_Q - s_Q T}{n_Q} \quad (2)$$

are the Gibbs energies per baryon (average chemical potentials) for the hadron and quark phase respectively, ε_H (ε_Q), P_H (P_Q), s_H (s_Q) and n_H (n_Q) denote respectively the total (*i.e.*, including leptonic contributions) energy density, total pressure, total entropy density, and baryon number density for the hadron (quark) phase.

Above the transition point P_0 (see Fig. 1) the hadronic phase is metastable, and the stable quark phase will appear as a result of a nucleation process. Virtual drops of the stable quark phase will arise from localized fluctuations in the state variables of the metastable hadronic phase. These fluctuations are characterized by a time scale

$\nu_0^{-1} \sim 10^{-23}$ s. This time scale is set by the strong interactions (which are responsible for the deconfinement phase transition), and it is many orders of magnitude shorter than the typical time scale for the weak interactions. Therefore quark flavor must be conserved forming a virtual drop of QM. We will refer to this form of deconfined matter, in which the flavor content is equal to that of the β -stable hadronic system at the same pressure and temperature, as the Q^* -phase. For example, if quark deconfinement occurs in β -stable nuclear matter (non-strange hadronic matter), it will produce a two-flavor (u and d) quark matter droplet having

$$n_u/n_d = (1 + x_p)/(2 - x_p), \quad (3)$$

n_u and n_d being the up and $down$ quark number densities respectively, and x_p the proton fraction in the β -stable hadronic phase. In the more general case in which the hadronic phase has a strangeness content (*e.g.*, hyperonic matter), the deconfinement transition will form a droplet of strange matter with a flavor content equal to that of the β -stable hadronic system at the same pressure, according to the relation:

$$\begin{pmatrix} x_u \\ x_d \\ x_s \end{pmatrix} = \begin{pmatrix} 2 & 1 & 1 & 2 & 1 & 0 & 1 & 0 \\ 1 & 2 & 1 & 0 & 1 & 2 & 0 & 1 \\ 0 & 0 & 1 & 1 & 1 & 1 & 2 & 2 \end{pmatrix} \begin{pmatrix} x_p \\ x_n \\ x_\Lambda \\ x_{\Sigma^+} \\ x_{\Sigma^0} \\ x_{\Sigma^-} \\ x_{\Xi^0} \\ x_{\Xi^-} \end{pmatrix}, \quad (4)$$

where $x_i = n_i/n$ are the concentrations of the different particle species.

Soon afterward a critical size drop of Q^* -matter is formed, the weak interactions will have enough time to act, changing the quark flavor fraction of the deconfined droplet to lower its energy, and a droplet of β -stable QM is formed (hereafter the Q -phase). This first seed of β -stable QM will trigger the conversion [62] of the pure hadronic star to a quark star (QS), *i.e.* to a hybrid neutron star or to a strange star [63, 64, 65, 66, 67, 68, 69, 70] depending on the details of the EOS for quark matter used to model the phase transition.

The direct formation by fluctuations of a drop of β -stable QM is also possible in principle. However, it is strongly suppressed with respect to the formation of the Q^* -phase drop by a factor $\sim G_F^{2N/3}$, being N the number of particles in the critical size quark drop and G_F the Fermi constant of weak interaction. This is so because the formation of a β -stable drop will imply the almost simultaneous conversion of $\sim N/3$ up and down quarks into strange quarks. For a critical size β -stable drop at the center of a neutron star it is found $N \sim 100 - 1000$, and therefore the suppression factor is actually very tiny.

In Fig. 2 we plot the Gibbs' energies per baryon for the hadron-phase and for the Q^* -phase in neutrino-free matter, at different temperatures ($T = 0, 10, 20, 30$ MeV). Results in Fig. 2 are obtained using the GM1 model with

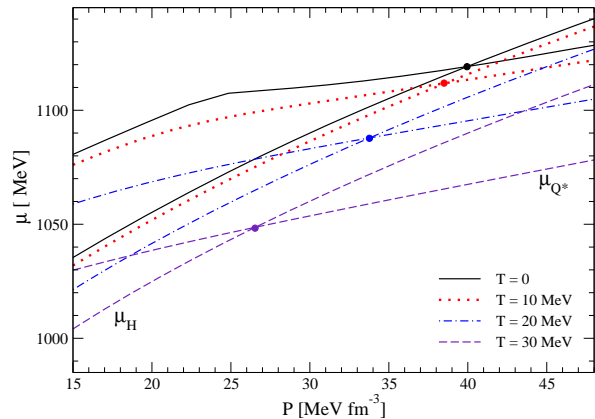


Fig. 2. (Color on line) Gibbs energy per baryon of β -stable hadronic phase and Q^* -phase, in neutrino-free matter, as a function of pressure, at different temperatures. Lines with the steeper slope refer to the hadronic phase. Full dots indicate the transition pressure P_0 for each temperature. GM1 EOS with $x_\sigma = 0.6$ for the hadronic phase and MIT bag model EOS with $B = 85$ MeV/fm³ for the Q^* -phase (GM1_{0.6}-B85 EOS).

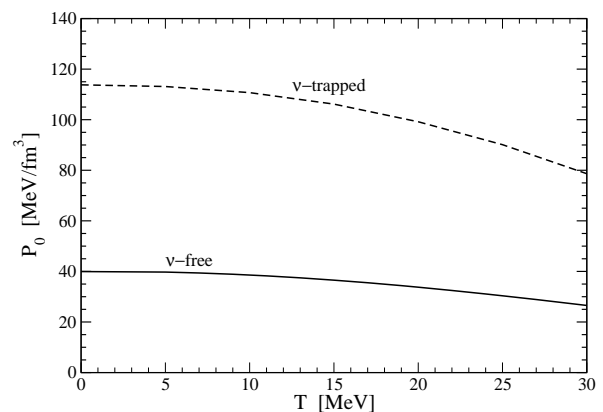


Fig. 3. Phase equilibrium curve between the β -stable hadronic phase and the Q^* phase. The continuous curve is relative to neutrino-free matter, the dashed curve to matter with trapped neutrinos. EOS: GM1 with $x_\sigma = 0.6$ plus MIT bag model with $B = 85$ MeV/fm³.

$x_\sigma = 0.6$ for the hadronic phase and the MIT bag model with $B = 85$ MeV/fm³ for the quark phase (hereafter the GM1_{0.6}-B85 EOS). Lines with the steeper slope refer to the hadron phase. As we see, the transition pressure P_0 (indicated by a full dot) decreases when the hadronic matter temperature is increased.

The phase equilibrium curve $P_0(T)$ between the β -stable hadronic phase and the Q^* -phase is shown in Fig. 3 for neutrino-free matter and matter with trapped neutrinos, making use of the GM1_{0.6}-B85 EOS. The region of the P_0 - T plane above each curve represents the deconfined Q^* -phase. As expected [71, 72, 35, 73] neutrino trapping in β -stable hadronic matter inhibits the quark deconfinement phase transition, thus the global effect of neutrino-

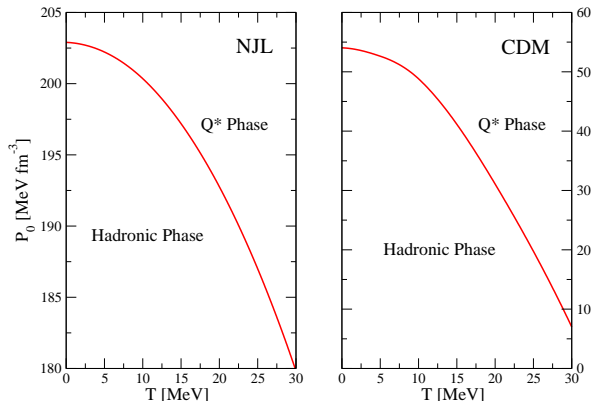


Fig. 4. Phase equilibrium curve between the β -stable hadronic phase and the Q^* -phase, neutrino-free matter. The EOS for the hadronic phase is obtained using the GM1 model with $x_\sigma = 0.7$, the EOS for the Q^* -phase using the NJL model (left panel) or the Chromo Dielectric model (right panel).

trapping is to produce a shift of the phase equilibrium curve toward higher values of the pressure in the P_0 - T plane.

In Fig. 4, we show the phase equilibrium curve, for neutrino-free matter, in the case of the NJL model (left panel) or the Chromo Dielectric model (right panel) to describe the deconfined phase. For the hadron phase we take the GM1 model with $x_\sigma = 0.7$ (GM1_{0.7}) in both cases. Notice that in the case of the NJL model the transition pressure $P_0(T)$ is substantially higher than the one in the case of the MIT bag or Chromo Dielectric models to describe the deconfined phase. As discussed in detail in Ref. [42], this behaviour can be traced back the large value of the strange quark effective mass in the NJL model.

As is well known, for a first-order phase transition the derivative dP_0/dT is related to the specific latent heat \mathcal{Q} of the phase transition by the Clapeyron-Clausius equation

$$\frac{dP_0}{dT} = -\frac{n_H n_{Q^*}}{n_{Q^*} - n_H} \frac{\mathcal{Q}}{T} \quad (5)$$

$$\mathcal{Q} = \tilde{W}_{Q^*} - \tilde{W}_H = T(\tilde{S}_{Q^*} - \tilde{S}_H) \quad (6)$$

where \tilde{W}_H (\tilde{W}_{Q^*}) and \tilde{S}_H (\tilde{S}_{Q^*}) denote the enthalpy per baryon and entropy per baryon for the hadron (quark) phase, respectively. The specific latent heat \mathcal{Q} and the hadron and quark baryon number densities n_H and n_{Q^*} at phase equilibrium are reported in Tables 1 and 2 in the case of the GM1_{0.6}-B85 equation of state. Results in Table 1 refer to neutrino-free matter, whereas those in Table 2 refer to matter with trapped neutrinos. As expected for a first-order phase transition, one has a discontinuity jump in the phase number densities: in our particular case $n_{Q^*}(T, P_0) > n_H(T, P_0)$. This result, together with the positive value of \mathcal{Q} (*i.e.* the deconfinement phase transition absorbs heat), tells us (see Eq. (5)) that the phase transition temperature decreases with pressure (as in the melting of ice).

Table 1. The specific (*i.e.* per baryon) latent heat \mathcal{Q} and the phase number densities n_H and n_{Q^*} at phase equilibrium. GM1 EOS with $x_\sigma = 0.6$ for the hadronic phase, MIT bag model with $B = 85$ MeV/fm³ for the quark phase. Results for neutrino-free matter.

T MeV	\mathcal{Q} MeV	n_{Q^*} fm ⁻³	n_H fm ⁻³	P_0 MeV/fm ³
0	0.00	0.453	0.366	39.95
5	0.56	0.451	0.364	39.74
10	2.40	0.447	0.358	38.58
15	5.71	0.439	0.348	36.55
20	10.60	0.428	0.334	33.77
25	17.17	0.414	0.316	30.36
30	25.44	0.398	0.294	26.53

Table 2. Same as Table 1, but with trapped neutrinos.

T MeV	\mathcal{Q} MeV	n_{Q^*} fm ⁻³	n_H fm ⁻³	P_0 MeV/fm ³
0	0.00	0.603	0.516	113.77
5	0.65	0.601	0.514	113.11
10	2.87	0.594	0.509	110.69
15	6.78	0.580	0.499	106.17
20	12.65	0.560	0.483	99.18
25	20.21	0.534	0.462	90.12
30	29.88	0.502	0.434	78.65

The effect of neutrino trapping on the phase equilibrium properties of the system can be seen comparing the results reported in Tables 1 and 2. As we see, the phase number densities n_H and n_{Q^*} at phase equilibrium are shifted to higher values, and the specific latent heat \mathcal{Q} is increased with respect to the neutrino-free matter case.

4 Quark matter nucleation in cold hadronic stars

Initially, we assume that the compact star survives the early stages of its evolution as a pure hadronic star, and we study quark matter nucleation in cold ($T = 0$) neutrino-free hadronic matter. The case of quark matter nucleation at finite temperature in neutrino-free and neutrino-trapped matter will be discussed in the Section 6.

In our scenario, we consider a purely hadronic star whose central pressure is increasing due to spin-down or due to mass accretion, *e.g.*, from a companion star. As the central pressure exceeds the deconfinement threshold value P_0 , a virtual drop of quark matter in the Q^* -phase can be formed in the central region of the star. As soon as a real drop of Q^* -matter is formed, it will grow very rapidly and the original Hadronic Star will be converted to an Hybrid Star or to a Strange Star, depending on the detail of the EOS for quark matter employed to model the phase transition.

In a cold ($T = 0$) and neutrino-free pure hadronic star the formation of the first drop of QM could take place

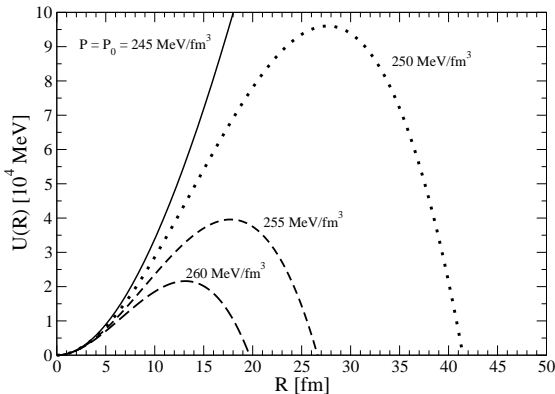


Fig. 5. Potential energy of the QM drop as a function of the radius of the drop for several pressures above P_0 at $T = 0$. The hadronic phase is described with the GM3 model whereas for the Q^* phases is employed the MIT bag model with $m_s = 150$ MeV, $B = 152.45$ MeV/fm³. The surface tension σ is taken equal to 30 MeV/fm².

solely via a quantum nucleation process. The basic quantity needed to calculate the nucleation time is the energy barrier separating the Q^* -phase from the metastable hadronic phase. This energy barrier, which represents the difference in the free energy of the system with and without a Q^* -matter droplet, can be written as [74,75]

$$U(\mathcal{R}) = \frac{4}{3}\pi n_{Q^*}(\mu_{Q^*} - \mu_H)\mathcal{R}^3 + 4\pi\sigma\mathcal{R}^2 \quad (7)$$

where \mathcal{R} is the radius of the droplet (supposed to be spherical), and σ is the surface tension for the surface separating the hadron from the Q^* -phase. The energy barrier has a maximum at the critical radius $\mathcal{R}_c = 2\sigma/[n_{Q^*}(\mu_H - \mu_{Q^*})]$. We neglected the term associated with the curvature energy and also the terms connected with the electrostatic energy, since they are known to only introduce small corrections [75,33]. The value of the surface tension σ for the interface separating the quark and hadron phase is poorly known, and typically values used in the literature range within 10 – 50 MeV fm⁻² [76]. Larger values of σ in the range 50–160 MeV fm⁻² have also been obtained in the literature [77,78]. Clearly these large values of the surface tension disfavor or inhibit quark matter nucleation in hadronic stars [50].

The nucleation time, *i.e.* the time needed to form the first drop of the Q^* -phase, can be straightforwardly evaluated within a semi-classical approach [75,31,32]. First one computes, in the Wentzel-Kramers-Brillouin (WKB) approximation, the ground state energy E_0 and the oscillation frequency ν_0 of the drop in the potential well $U(\mathcal{R})$. Then, the probability of tunneling is given by

$$p_0 = \exp\left[-\frac{A(E_0)}{\hbar}\right] \quad (8)$$

where A is the action under the potential barrier which in a relativistic framework reads

$$A(E) = \frac{2}{c} \int_{\mathcal{R}_-}^{\mathcal{R}_+} \sqrt{[2\mathcal{M}(\mathcal{R})c^2 + E - U(\mathcal{R})][U(\mathcal{R}) - E]} d\mathcal{R}, \quad (9)$$

with \mathcal{R}_{\pm} the classical turning points and

$$\mathcal{M}(\mathcal{R}) = 4\pi\rho_H \left(1 - \frac{n_{Q^*}}{n_H}\right)^2 \mathcal{R}^3 \quad (10)$$

the droplet effective mass, with ρ_H and n_H the hadron energy density and the hadron baryon number density, respectively. The nucleation time is then equal to

$$\tau_q = (\nu_0 p_0 N_c)^{-1}, \quad (11)$$

where $N_c \sim 10^{48}$ is the number of nucleation centers expected in the innermost part ($r \leq R_{nuc} \sim 100$ m) of the HS, where the pressure and temperature (when we will consider the finite T case) can be considered constant and equal to their central values. The uncertainty in the value of N_c is expected to be within one or two orders of magnitude. In any case, all the qualitative features of our scenario will not be affected by this uncertainty [31,32,33].

As a consequence of the surface effects it is necessary to have an overpressure $\Delta P = P - P_0 > 0$ with respect to the bulk transition point P_0 to create a drop of deconfinement quark matter in the hadronic environment. The higher the overpressure, the easier to nucleate the first drop of Q^* matter. In other words, the higher the mass of the metastable pure hadronic star, the shorter the time to nucleate a quark matter drop at the center of the star.

As an illustrative example, we plot in Fig. 5 the potential energy $U(\mathcal{R})$ for the formation of a quark matter droplet for different values of the stellar central pressure P_c above the deconfinement threshold value P_0 . The curves in Fig. 5 are relative to a given set of EOS for the two phases of dense matter and to a fixed value of the surface tension σ (see figure caption). As expected the potential barrier is lowered as central pressure increases.

Thus a pure hadronic star, having a central pressure P_c larger than the transition pressure P_0 for the formation of the Q^* -phase, is metastable [31,32,33] to the “decay” (conversion) to a quark star (QS) *i.e.* to a stellar configuration in which deconfined quark matter is present.

These metastable HSs have a *mean-life time* which is related to the nucleation time to form the first critical-size drop of deconfined matter in their interior (the actual *mean-life time* of the HS will depend on the mass accretion or on the spin-down rate which modifies the nucleation time via an explicit time dependence of the stellar central pressure). Following Refs. [31,32,33] we define as *critical mass* M_{cr} of the metastable HSs, the value of the gravitational mass for which the nucleation time is equal to one year: $M_{cr} \equiv M^{HS}(\tau_q = 1\text{yr})$. Pure hadronic stars with $M^{HS} > M_{cr}$ are very unlikely to be observed. Thus M_{cr} plays the role of an *effective maximum mass* [33] for the hadronic branch of compact stars. Notice that

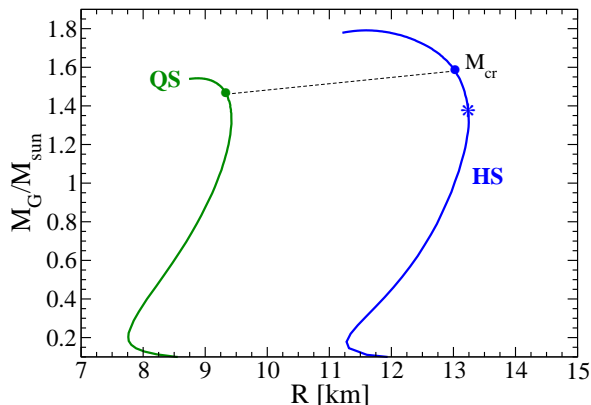


Fig. 6. (Color on line) Mass-radius relation for pure hadronic star (HS) and hybrid star (QS) configurations. The configuration marked with an asterisk represents the HS for which $\tau_q = \infty$ (*i.e.* $P_c = P_0$). The conversion process of the HS, with a gravitational mass equal to M_{cr} , into the final QS is denoted by the full circles connected by a dashed line. Results are relative to the GM1 model with $x_\sigma = 0.6$ for the hadronic phase and the MIT bag model EOS with $B = 85$ MeV/fm³ for the quark phase. The surface tension is $\sigma = 30$ MeV/fm². Stellar masses are in unit of the mass of the sun, $M_{sun} = 1.989 \times 10^{33}$ g.

the Oppenheimer–Volkoff [79] maximum mass M_{max}^{HS} is determined by the overall stiffness of the EOS for hadronic matter, whereas the value of M_{cr} will depend in addition on the bulk properties of the EOS for quark matter and on the properties at the interface between the confined and deconfined phases of matter (*e.g.*, the surface tension σ).

These findings are exemplified in Fig. 6, where we show the mass-radius (MR) curve for hadronic stars (HS) and that for quark stars (QS). The configuration marked with an asterisk on the hadronic MR curve represents the HS for which the central pressure is equal to P_0 and thus $\tau_q = \infty$. The full circle on the HS sequence represents the critical mass configuration M_{cr} , in the case $\sigma = 30$ MeV/fm². The full circle on the QS mass-radius curve represents the hybrid star which is formed from the conversion of the hadronic star with $M^{HS} = M_{cr}$. We assume [62] that during the stellar conversion process the total number of baryons in the star (or in other words the stellar baryonic mass M_B) is conserved. Thus the total energy liberated in the stellar conversion is given by [62] the difference between the gravitational mass of the initial hadronic star ($M_{in} \equiv M_{cr}$) and that of the final quark star M_{fin} configuration with the same baryonic mass (*i.e.* with $M_{B,cr} = M_{B,fin}$):

$$E_{conv} = (M_{in} - M_{fin})c^2. \quad (12)$$

It has been shown [62, 31, 32, 33, 36, 37, 38] (see also Tabs. 3 and 4) that $E_{conv} = 0.5\text{--}4.0 \times 10^{53}$ erg. This huge amount of released energy will cause a powerful neutrino burst, likely accompanied by intense gravitational waves emission, and conceivably it could cause a second delayed

explosion¹. Under favorable physical conditions this second explosion could be the energy source of a powerful gamma-ray burst (GRB) [31, 32]. Thus this scenario is able to explain a “delayed” connection between supernova explosions and GRBs.

It has also been suggested [80] that the delayed stellar conversion process of a pure HS to a QS, can impart a second kick to the nascent QS with respect to the first kick imparted to the newly formed HS during the supernova explosion. Thus this model [80] could explain in a natural way the observed bimodal distribution of the kick velocities of radio pulsars [81]. Thus, according to the authors of Ref. [80], the low velocity component of the pulsar velocity distribution receives contributions mainly from hadronic stars which have passed through a single explosion (the supernova explosion). The high velocity component is mostly composed of quark stars which have received a second kick due to the energy release associated to the stellar conversion process.

The last stages of the evolution of a massive star ($M > 8 M_{sun}$), within the scenario proposed by the authors of Ref. [31, 32], are schematically depicted in Fig. 7.

In Fig. 8 we show the mass-radius relation in the case of the GM1 EOS for two different values of the hyperon coupling ($x_\sigma = 0.6$ and 0.8) and for two different values of the bag constant ($B = 75$ and 100 MeV/fm³). These results illustrate that the outcome of the scenario proposed in Ref. [31, 32], and, in particular, the final fate of the critical mass HS, depends on the details of the EOS describing the two matter phases. Specifically, as shown in Fig. 8, for some values of the EOS parameters, the critical mass HS will collapse to a black hole (BH) for the reason that the baryonic mass of the critical mass configuration is larger than the maximum baryonic mass for the quark star sequence (*i.e.* $M_{B,cr} > M_{B,max}^{QS}$).

In Tables 3 and 4, we report the calculated values of the critical gravitational (baryonic) mass M_{cr} ($M_{B,cr}$), the value of mass of the final QS configuration M_{fin} and the energy E_{conv} released in the stellar conversion process. The results are relative to the GM1 model with $x_\sigma = 0.7$ for the hadronic phase and to the extended bag model EOS of Ref. [56, 57, 58] for the quark phase, using different values for the effective bag constant B_{eff} and the perturbative QCD correction term a_4 . The results in Tab. 3 are relative to a surface tension $\sigma = 10$ MeV/fm², whereas those in Tab. 4 to $\sigma = 30$ MeV/fm². Notice that for these EOS models and for the parameters reported in Tables 3 and 4, both the critical mass of the hadronic star sequence and the maximum mass M_{max}^{QS} of the quark star sequence are consistent with present measured neutron star masses and, in particular, with the mass $M = 1.97 \pm 0.04 M_{sun}$ of PSR J1614-2230 [82] and $M = 2.01 \pm 0.04 M_{sun}$ of PSR J0348+0432 [83].

The mass-radius relation for the stellar configurations relative to the entry of the last row of Tab. 3 is pre-

¹ delayed with respect to the first explosion, *i.e.* the supernova explosion, which formed the hadronic star (“neutron star”). In other words, we assume (in this section) that quark matter is not formed during the stellar collapse generating the

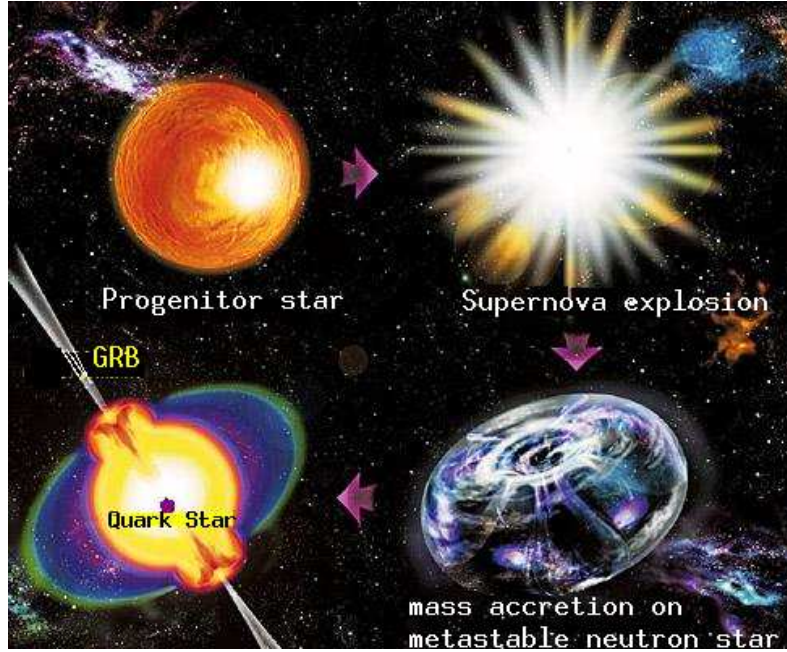


Fig. 7. (Color on line) A schematic representation of the last stages of the evolution of a massive star ($M > 8 M_{sun}$) leading to the delayed conversion of a pure hadronic star to a quark star (hybrid or strange star) and to the emission of a neutrino burst and possibly to a gamma ray burst [31,32]. Clockwise from the upper left corner of the figure: (i) nuclear burning stage of the progenitor star; (ii) supernova explosion and birth of a pure hadronic star (“neutron star”); (iii) mass accretion on the metastable hadronic star; (iv) conversion process of the hadronic star to a quark star (second “explosion”) neutrino burst and gamma ray burst.

Table 3. Critical mass and energy released in the conversion process of an HS into a QS. Results are relative to the GM1 model with $x_\sigma = 0.7$ for the hadronic phase and the extended bag model EOS of Ref. [56,57,58] for the quark phase, using different values for the effective bag constant B_{eff} and the perturbative QCD correction term a_4 . For the quark masses we use $m_s = 100$ MeV, $m_u = m_d = 0$. The value of the critical gravitational (baryonic) mass of the HS sequence is reported on the column labeled M_{cr} ($M_{B,cr}$), whereas those of the mass of the final QS formed in the stellar conversion process of the critical mass HS are shown on the column labeled M_{fin} . The column labeled M_{max}^{QS} denotes the maximum gravitational mass of the QS sequence. Finally the energy released in the stellar conversion process are shown on the column labeled E_{conv} . Units of B_{eff} and σ are MeV/fm^3 and MeV/fm^2 respectively. All stellar masses are given in units of the mass of the sun, $M_{sun} = 1.989 \times 10^{33}$ g, and E_{conv} is given in units of 10^{53} erg. The surface tension is $\sigma = 10 \text{ MeV}/\text{fm}^2$.

B_{eff}	a_4	M_{cr}	$M_{B,cr}$	M_{fin}	M_{max}^{QS}	E_{conv}
37.63	0.65	2.003	2.312	1.848	2.318	2.77
50.72	0.65	2.033	2.354	1.954	2.013	1.41
41.14	0.70	1.891	2.158	1.731	2.229	2.86
47.20	0.70	1.940	2.225	1.814	2.088	2.25

supernova explosion and the protohadronic star. This possibility will be discussed in Section 6.

Table 4. Same as Table 3, but for a value of the surface tension $\sigma = 30 \text{ MeV}/\text{fm}^2$.

B_{eff}	a_4	M_{cr}	$M_{B,cr}$	M_{fin}	M_{max}^{QS}	E_{conv}
37.63	0.65	2.021	2.328	1.859	2.318	2.90
50.72	0.65	2.039	2.362	1.960	2.013	1.41
41.14	0.70	1.995	2.301	1.832	2.229	2.91
47.20	0.70	1.973	2.270	1.846	2.088	2.27

sented in Fig. 9. As we can see, for this EOS parametrization, PSR B1913+16 (which has a mass $M = 1.4398 \pm 0.0002 M_{sun}$ [84]) can be interpreted as a pure HS, whereas PSR J1614-2230 is more likely a QS.

The stellar conversion process, described so far, will start to populate the new branch of quark stars, *i.e.* the part of the QS sequence above the full circle (see Fig. 6 and 9). Long term accretion on the QS can next produce stars with masses up to the maximum mass M_{max}^{QS} for the quark star configurations. Thus within this scenario one has two coexisting families of compact stars: pure hadronic stars and quark stars [33] (see [85] in this Topical Issue). The quark star branch is occasionally referred to as the “third family” of compact stars, considering white dwarfs as the first family and pure hadronic stars as the second family. Notice also that there is a range of values of stellar gravitational mass (see Fig. 6 and 9) where hadronic stars

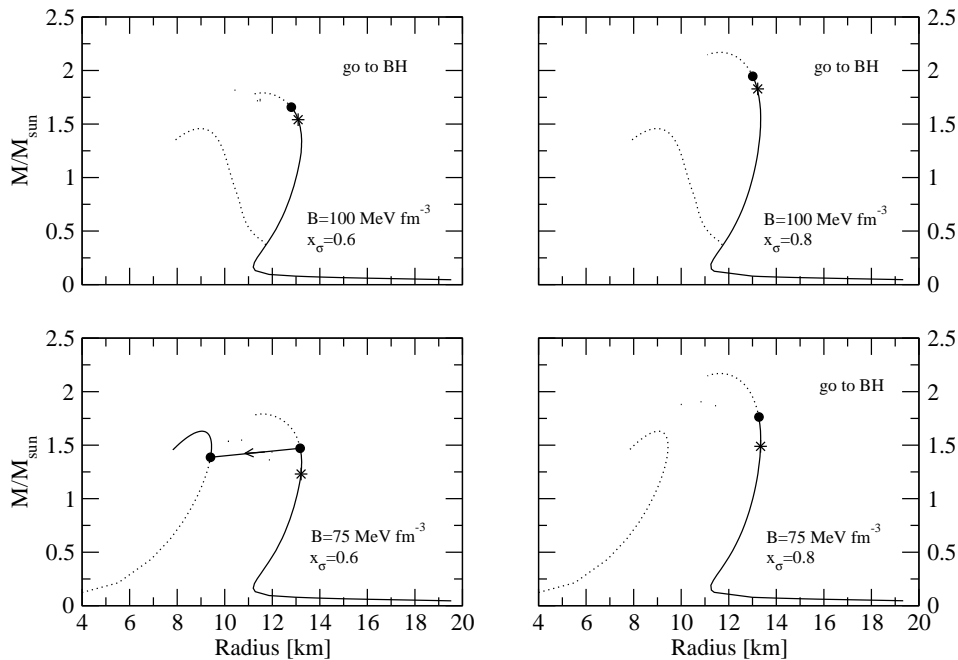


Fig. 8. Mass-radius relation for a pure HS described within the GM1 parametrization and that of the hybrid stars or strange stars configurations for two values of the bag constant ($B = 75$ and 100 MeV/fm^3) and two values of the hyperon-meson coupling ($x_\sigma = 0.6$, and 0.8) and $m_s = 150 \text{ MeV}$. The configuration marked with an asterisk represents in all cases the HS for which the central pressure is equal to P_0 . The conversion process of the HS, with a gravitational mass equal to M_{cr} , into a final hybrid star or strange star is denoted by the full circles connected by an arrow. The label "go to BH" designates the case in which the critical mass HS collapses to a black hole. In all the panels σ is taken equal to 30 MeV/fm^2 .

and quark stars with the same gravitational mass can exist ("twin stars").

5 The limiting mass of compact stars: extending the Oppenheimer-Volkoff mass limit concept

The possibility to have metastable hadronic stars, together with the predicted coexistence of two distinct families of compact stars, demands an extension of the concept of maximum mass of a "neutron star" with respect to the *classical* one introduced by Oppenheimer and Volkoff in 1939 [79]. Since metastable HS with a "short" *mean-life time* are very unlikely to be observed, the extended concept of maximum mass must be introduced in view of the comparison with the values of the mass of compact stars deduced from direct astrophysical observation. Having in mind this operational definition, the authors of Ref. [33] called *limiting mass* of a compact star, and denoted it as M_{lim} , the physical quantity defined in the following way: (a) if the nucleation time $\tau(M_{max}^{HS})$ associated to the maximum mass configuration for the hadronic star sequence is of the same order or much larger than the age of the universe T_{univ} , then

$$M_{lim} = M_{max}^{HS}, \quad (13)$$

in other words, the limiting mass in this case coincides with the Oppenheimer - Volkoff maximum mass for the hadronic star sequence.

(b) If the critical mass M_{cr} is smaller than M_{max}^{HS} (*i.e.* $\tau(M_{max}^{HS}) < 1 \text{ yr}$), thus the limiting mass for compact stars is equal to the largest value between the critical mass for the HS and the maximum mass for the quark star (HyS or SS) sequence

$$M_{lim} = \max[M_{cr}, M_{max}^{QS}]. \quad (14)$$

(c) Finally, one must consider an "intermediate" situation for which $1 \text{ yr} < \tau(M_{max}^{HS}) < T_{univ}$. As the reader can easily realize, now

$$M_{lim} = \max[M_{max}^{HS}, M_{max}^{QS}], \quad (15)$$

depending on the details of the EOS which could give $M_{max}^{HS} > M_{max}^{QS}$ or vice versa.

6 Quark matter nucleation in proto-hadronic stars

A neutron star at birth (proto-neutron star) is very hot ($T = 10 - 30 \text{ MeV}$) with neutrinos being still trapped in the stellar interior [86, 87, 71, 88, 89, 90]. Subsequent neutrino diffusion causes deleptonization and heats the stellar matter to an approximately uniform entropy per baryon $\tilde{S} = 1$

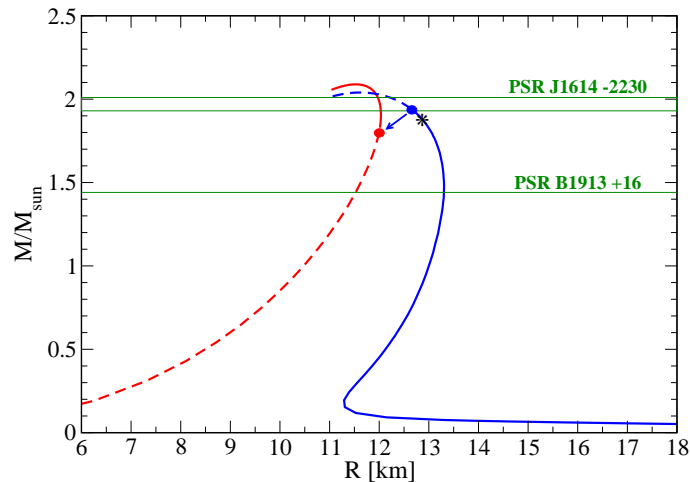


Fig. 9. (Color on line) Mass-radius relation for a pure HS described within the GM1 model of hyperonic matter with hyperon- σ meson coupling $x_\sigma = 0.7$, and for strange star configurations with the extended bag model EOS of Ref. [56,57,58] with $B_{eff} = 47.2 \text{ MeV/fm}^3$ and $a_4 = 0.7$. The configuration marked with an asterisk represents the HS for which $\tau_q = \infty$. The conversion process of the HS, with a gravitational mass equal to M_{cr} , into the final QS is denoted by the full circles connected by an arrow. The values of the critical gravitational (baryonic) mass and of the final QS mass are calculated for a surface tension $\sigma = 10 \text{ MeV/fm}^2$. Their numerical values are given in the last row of Tab. 3. The lower horizontal line represents the mass $M = 1.4398 \pm 0.0002 M_{sun}$ [84] of the pulsar PSR B1913+16, whereas the higher horizontal lines represent the mass $M = 1.97 \pm 0.04 M_{sun}$ of PSR J1614-2230 [82].

-2 (in units of the Boltzmann's constant k_B). Depending on the stellar composition, during this stage neutrino escape can lead the more “massive” stellar configurations to the formation of a black hole [91,71]. However, if the mass of the star is sufficiently small, the star will remain stable and it will cool to temperatures well below 1 MeV within a cooling time $t_{cool} \sim$ a few 10^2 s, as the neutrinos continue to carry energy away from the stellar material [86,71,88]. Thus in a proto-neutron star, the quark deconfinement phase transition will be likely triggered by a thermal nucleation process [92,93,94,95]. In fact, for sufficiently high temperatures, thermal nucleation is a much more efficient process with respect to the quantum nucleation mechanism.

In Ref. [39,41] we established the physical conditions under which a newborn hadronic star (proto-hadronic star, PHS) could survive the early stages of its evolution without “decaying” to a quark star.

According to the Langer theory [96,97] of homogeneous nucleation the thermal nucleation rate can be written [97] as

$$I = \frac{\kappa}{2\pi} \Omega_0 \exp(-U(\mathcal{R}_c, T)/T) \quad (16)$$

where κ is the so-called dynamical prefactor, which is related to the growth rate of the drop radius \mathcal{R} near the critical radius (\mathcal{R}_c), and Ω_0 is the so-called statistical prefactor, which measures the phase-space volume of the saddle-point region around \mathcal{R}_c . We have used [39,41] for κ and Ω_0 the expressions derived in Refs. [98,99], where the Langer nucleation theory has been extended to the case of first order phase transitions occurring in relativistic systems, as in the case of the quark deconfinement transition. The

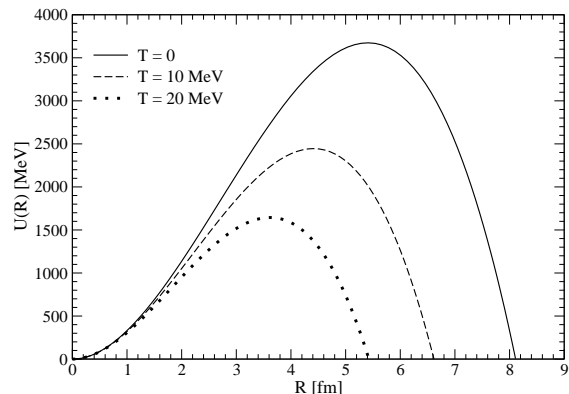


Fig. 10. Energy barrier for a virtual drop of the Q^* -phase in β -stable neutrino-free hadronic matter as a function of the droplet radius and for different temperatures for a fixed pressure $P = 57 \text{ MeV/fm}^3$. Results are relative to the GM1_{0.6}-B85 equation of state and surface tension $\sigma = 30 \text{ MeV/fm}^2$.

dominant factor in the nucleation rate (16) is the exponential, in which $U(\mathcal{R}_c, T)$ is the activation energy, *i.e.* the change in the free energy of the system required to activate the formation of a critical size droplet. This quantity has been calculated [39,41] using the generalization of Eq. (7) to the case of $T \neq 0$ (thus using finite temperature EOS for the hadronic and the quark phases), and assuming a temperature independent surface tension.

The thermal nucleation time τ_{th} , relative to the innermost stellar region ($V_{nuc} = (4\pi/3)R_{nuc}^3$, with $R_{nuc} \sim 100$ m) where almost constant pressure and temperature oc-

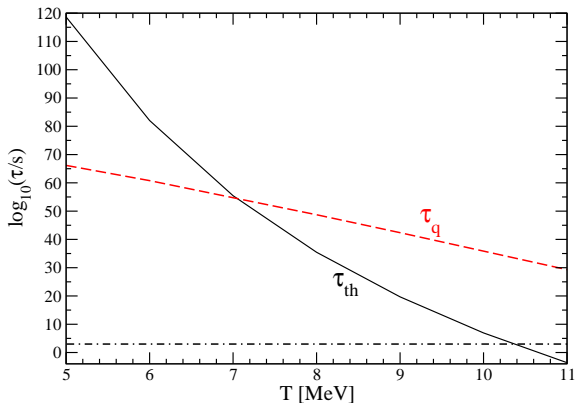


Fig. 11. (Color on line) Thermal (τ_{th}) and quantum (τ_q) nucleation time of quark matter (Q*-phase) in β -stable neutrino-free hadronic matter as a function of temperature at fixed pressure $P = 57 \text{ MeV}/\text{fm}^3$. The crossover temperature is $T_{co} = 7.05 \text{ MeV}$. The limiting conversion temperature for the proto-hadronic star is, in this case, $\Theta = 10.3 \text{ MeV}$, obtained from the intersection of the thermal nucleation time curve (continuous line) and the dot-dashed line representing $\log_{10}(\tau/s) = 3$. The surface tension is $\sigma = 30 \text{ MeV}/\text{fm}^2$. Results are relative to GM1_{0.6}-B85 EOS.

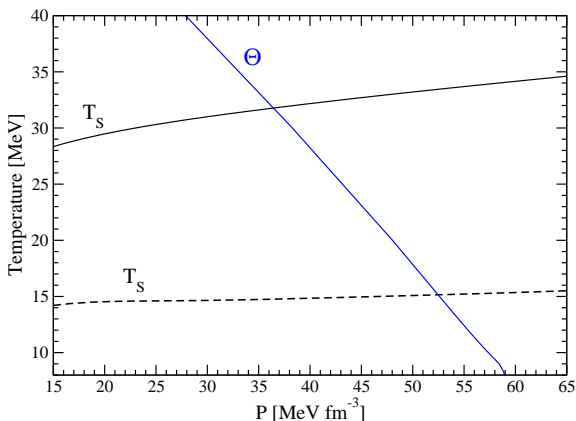


Fig. 12. (Color on line) The limiting conversion temperature Θ for a newborn hadronic star as a function of the central stellar pressure. Newborn hadronic stars with a central temperature and pressure located on the right side of the curve $\Theta(P)$ will nucleate a Q*-matter drop during the early stages of their evolution, and will finally evolve to cold and deleptonized quark stars, or will collapse to black holes. The lines labeled T_s represent the stellar matter temperature as a function of pressure at fixed entropies per baryon $\tilde{S}/k_B = 1$ (dashed line) and 2 (solid line). Results are relative to GM1_{0.6}-B85 EOS.

cur, can thus be written as

$$\tau_{th} = (V_{nuc} I)^{-1}. \quad (17)$$

In Fig. 10, we represent the energy barrier for a virtual drop of the Q*-phase in the neutrino-free hadronic phase as a function of the droplet radius and for different temperatures at a fixed pressure $P = 57 \text{ MeV}/\text{fm}^3$. Results

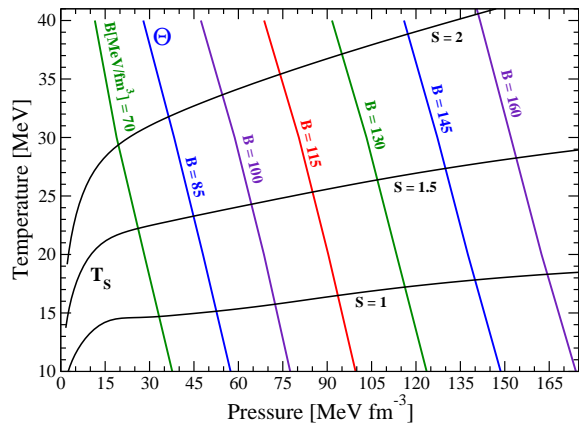


Fig. 13. (Color on line) The limiting conversion temperature Θ for a newborn hadronic star as a function of the central stellar pressure for different values of the bag constant B . The lines labeled T_s represent the stellar matter temperature as a function of pressure at fixed entropies per baryon $\tilde{S}/k_B = 1, 1.5, 2$. Results for neutrino-free matter.

in Fig. 10 are obtained using the GM1_{0.6}-B85 equation of state. As expected, from the results plotted in Fig. 2, the energy barrier $U(\mathcal{R}, T)$ and the droplet critical radius \mathcal{R}_c decrease as the matter temperature is increased. This effect favors the Q*-phase formation and, in particular, increases (decreases) the quantum nucleation rate (nucleation time τ_q) with respect to the corresponding quantities calculated at $T = 0$.

In Fig. 11, we plot the quantum and thermal nucleation times of the Q*-phase in β -stable neutrino-free hadronic matter as a function of temperature and at a fixed pressure $P = 57 \text{ MeV}/\text{fm}^3$. As expected, we find a crossover temperature T_{co} above which thermal nucleation is dominant with respect to the quantum nucleation mechanism. For the case reported in Fig. 11, we have $T_{co} = 7.05 \text{ MeV}$ and the corresponding nucleation time is $\log_{10}(\tau/s) = 54.4$.

Having in mind the physical conditions in the interior of a PHS [86,71], to establish if this star will survive the early stages of its evolution without decaying to a quark star, one has to compare the quark matter nucleation time $\tau = \min(\tau_q, \tau_{th})$ with the cooling time $t_{cool} \sim \text{a few } 10^2 \text{ s}$. If $\tau \gg t_{cool}$ then quark matter nucleation will not likely occur in the newly formed star, and this star will evolve to a cold deleptonized configuration. We thus introduce the concept of *limiting conversion temperature* Θ for the proto-hadronic star and define it as the value of the stellar central temperature T_c for which the Q*-matter nucleation time is equal to 10^3 s . The limiting conversion temperature Θ will clearly depend on the value of the stellar central pressure (and thus on the value of the stellar mass).

The limiting conversion temperature Θ is plotted in Fig. 12 as a function of the stellar central pressure. A proto-hadronic star with a central temperature $T_c > \Theta$ will likely nucleate a Q*-matter drop during the early

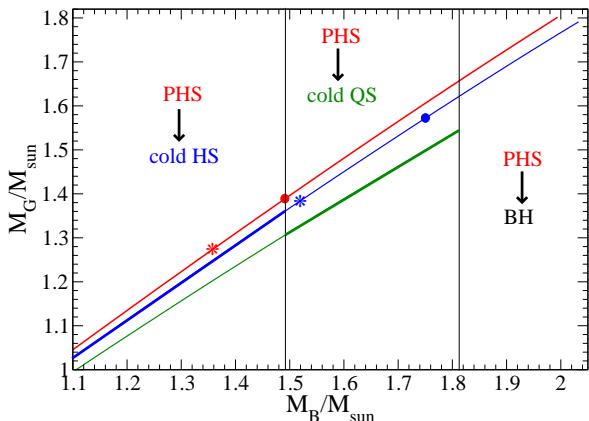


Fig. 14. (Color on line) Stellar equilibrium sequences in the gravitational–baryonic mass plane for the GM1_{0.6}–B85 EOS and $\sigma = 30$ MeV/fm². The upper (red) line represents the PHS sequence ($\tilde{S} = 2 k_B$). The middle (blue) line represents the cold HS sequence. The asterisk and the full circle on these lines represent respectively the stellar configuration with $\tau = \infty$ and the critical mass configuration M_{cr} . The lower (green) line represent the cold QS sequence. Assuming $M_B = \text{const}$, the evolution of a PHS in this plane occurs along a vertical line.

stages of its evolution, and will finally evolve to a cold and deleptonized quark star, or will collapse to a black hole (depending on the value of the stellar baryonic mass M_B and on the EOS).

In Fig. 13 we plot the limiting conversion temperature Θ for a newborn HS for different values of the bag constant. The increase in B produces a growth of the region of the P – T plane where the proto-hadronic star could survive Q^* nucleation and thus evolve to a cold hadronic star.

For an isentropic stellar core [86, 71], the central temperature of the proto-hadronic star is given, for the GM1_{0.6} EOS model, by the lines labeled by T_S in Fig. 12, relative to the case $\tilde{S} = 1 k_B$ (dashed curve) and $\tilde{S} = 2 k_B$ (continuous curve). The intersection point (P_S, Θ_S) between the two curves $\Theta(P)$ and $T_S(P)$ thus gives the central pressure and temperature of the configuration that we denote as the *critical mass* configuration of the proto-hadronic stellar sequence. Taking $\sigma = 30$ MeV/fm² and $\tilde{S} = 2 k_B$ we get $M_{cr} = 1.390 M_{sun}$ for the gravitational critical mass and $M_{B,cr} = 1.492 M_{sun}$ for the baryonic critical mass (being $M_{sun} = 1.989 \times 10^{33}$ g the mass of the sun).

The evolution of a PHS within our scenario is delineated in Fig. 14, where we plot the appropriate stellar equilibrium sequences in the gravitational–baryonic mass plane for the GM1_{0.6}–B85 EOS and $\sigma = 30$ MeV/fm². The upper (red) line represents the PHS sequence, *i.e.* isentropic HSs ($\tilde{S} = 2 k_B$) and neutrino-free matter. The middle (blue) line represents the cold HS sequence. The asterisk and the full circle on these lines represent respectively the stellar configuration with $\tau = \infty$ and the critical mass configuration. Finally, the lower (green) line represent the cold QS sequence. We assume $M_B = \text{const}$

during these stages of the stellar evolution. Thus according to the results in Fig. 14, proto-hadronic stars with a baryonic mass $M_B < 1.492 M_{sun}$ will survive Q^* -matter *early nucleation* (*i.e.* nucleation within the cooling time $t_{cool} \sim$ a few 10^2 s) and in the end they will form stable ($\tau = \infty$) cold hadronic stars. Proto-hadronic stars with $1.492 M_{sun} \leq M_B < 1.813 M_{sun}$ (the maximum baryonic mass $M_{B,max}^{QS}$ of the cold QS sequence for the present EOS) will experience early nucleation of a Q^* -matter drop and will ultimately form a cold deleptonized quark star. The last possibility is for PHSs having $M_B > 1.813 M_{sun}$. In this case the early nucleation of a Q^* -matter drop will trigger a stellar conversion process to a cold QS configuration with $M_B > M_{B,max}^{QS}$, thus these PHSs will finally form black holes.

The outcomes of this scenario are not altered by neutrino trapping effects in hot β -stable hadronic matter. In fact, for proto-hadronic stars with trapped neutrinos (ν PHSs) (with a lepton fraction $Y_L = 0.4$ and $\tilde{S} = 2 k_B$) we find [41] (for the same EOS and surface tension σ used in Fig. 14) a critical baryonic mass $M_{B,cr} = 1.96 M_{sun}$. Thus ν PHSs with $M_B \geq M_{B,cr}$ after neutrino escape and cooling will finally evolve to black holes. The fate of a ν PHS with $M_B < M_{B,cr}$ is the same as the corresponding neutrino-free PHS with equal baryonic mass.

In Fig. 15 we plot the PHS, cold HS, and cold QS sequences in the gravitational–baryonic mass plane for the case of the NJL model for the quark phase and the GM1 model in the case of pure nucleonic matter (right panel) or hyperonic matter with $x_\sigma = 0.7$ (left panel). It is clearly seen that in the case of the NJL model it is almost impossible to populate the QS branch. Cold quark stars can be formed in the case of $x_\sigma = 0.7$ (left panel) for a very narrow range of baryonic stellar masses $2.20 < M_B/M_{sun} < 2.23$.

In summary, proto-hadronic stars with a gravitational mass lower than the critical mass M_{cr} could survive the early stages of their evolution without decaying to a quark star [39, 41]. This outcome contrasts with the predictions of the earlier studies [92, 93, 94, 95] where it was inferred that all the pure hadronic compact stars, with a central temperature above 2–3 MeV, are converted to quark stars within the first seconds after their birth. However, the prompt formation of a critical size drop of quark matter could occur when $M > M_{cr}$. These proto-hadronic stars evolve to cold and deleptonized quark stars or collapse to a black holes [39, 41].

Finally, if quark matter nucleation occurs during the post-bounce stage of core-collapse supernova, then the quark deconfinement phase transition could trigger a delayed supernova explosion characterized by a peculiar neutrino signal [100, 49, 101, 102].

7 Conclusions

In the present review, which mainly summarizes the research reported in Ref. [31, 32, 33, 34, 35, 36, 37, 38, 39, 40, 41, 42, 43, 44], we have investigated the consequences of

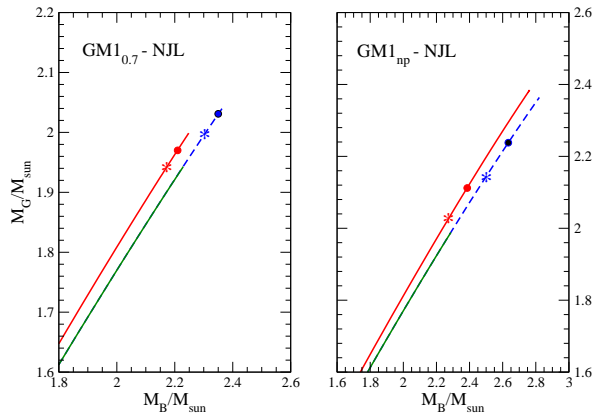


Fig. 15. (Color on line) Same as in the previous figure but in the case of the NJL model for the quark phase and the Glendenning–Moszkowski model for hyperonic matter with $x_\sigma = 0.7$ (GM1_{0.7}) (left panel) and pure nucleonic matter GM1_{np} (right panel).

the quark deconfinement phase transition in stellar compact objects when finite size effects between the deconfined quark phase and the hadronic phase are taken into account considering a first order phase transition.

We have found that above a threshold value of the gravitational mass a pure hadronic star is metastable to the decay (conversion) to a quark star. We have calculated the *mean-life time* of these metastable stellar configurations, the critical mass for the hadronic star sequence, and have explored how these quantities depend on the details of the EOS for dense matter. We have exposed how to extend [33] the concept of limiting mass of compact stars, with respect to the classical one given by Oppenheimer and Volkoff [79].

The stellar conversion of a HS to a QS liberates an energy of the order of 10^{53} erg and will cause a powerful neutrino burst, likely accompanied by intense gravitational waves emission, and conceivably it could cause a second delayed explosion (with respect to the supernova explosion, which formed the hadronic star). Under opportune physical conditions this second explosion could be the energy source of a powerful gamma-ray burst [31, 32]. This scenario is thus able to explain a “delayed” connection between supernova explosions and GRBs [31, 32]. It could also explain [80] in a natural way the observed bimodal distribution of the kick velocities of radio pulsars [81].

In addition, within the scenario discussed in the present review, one has two coexisting families of compact stars: pure hadronic stars and quark stars [31, 32, 33] (see also the contribution of Drago *et al.* in this Topical Issue). The members of these two families could have similar values for their gravitational masses but different values for their radii.

The advanced and innovative instruments on board of the new generation of X-ray satellites, as the Astrosat satellite (Indian Space Research Organization, which has

been launched on September 28th 2015), or on board of the NICER satellite (NASA, launch scheduled for October 2016) will be able to determine neutron star radii with high precision (*i.e.* better than 1 km uncertainty). Thus accurate measurements of both the mass and radius of a few individual “neutron stars” [103, 104] or measurements of temperature profiles of accretion discs around rapidly spinning compact stars [105] could shed light on the validity of the scenario discussed in the present work.

Acknowledgments

This work is partly supported by NewCompstar, COST Action MP1304.

References

1. J.M. Lattimer, M. Prakash, *Astrophys. Jour.* **550**, 426 (2001).
2. G.X. Peng, A. Li, U. Lombardo, *Phys. Rev. C* **77**, 065807 (2008).
3. Z.H. Li, H.-J. Schulze, *Phys. Rev. C* **78**, 028801 (2008).
4. C. Bernard *et al.*, *Phys. Rev. D* **71**, 034504 (2005).
5. M. Cheng *et al.*, *Phys. Rev. D* **74**, 054507 (2006).
6. Y. Aoki, G. Endrodi, Z. Fodor, S. D. Katz, and K. K. Szabó, *Nature* **443**, 675, (2006).
7. Y. Nambu, G. Jona-Lasinio, *Phys. Rev.* **122**, 345 (1961).
8. M. Buballa, *Phys. Rep.* **407**, 205 (2005).
9. P.N. Meisinger, M.C. Ogilvie, *Phys. Lett. B* **379**, 163 (1996).
10. K. Fukushima, *Phys. Lett. B* **591**, 277 (2004).
11. C. Ratti, M.A. Thaler, W. Weise, *Phys. Rev. D* **73**, 014019 (2006).
12. D. Blaschke, M. Buballa, A.E. Radzhabov, M.K. Volkov, *Phys. At. Nucl.* **71**, 1981 (2008).
13. G.A. Contrera, D. Gómez Dumm, N.N. Scoccola, *Phys. Lett. B* **661**, 113 (2008).
14. D. Blaschke, J. Berdermann, R. Lastowiecki, *Prog. Theor. Phys. Suppl.* **186**, 81 (2010).
15. V.A. Dexheimer, S. Schramm, *Nucl. Phys. B (Proc. Suppl.)* **199**, 319 (2010).
16. H. Gie, *Lecture Notes in Phys.* **852**, 287 (2012).
17. S.D.H. Hsu, M. Schwetz, *Phys. Lett. B* **432**, 203 (1998).
18. Z. Fodor, S.D. Katz, *JHEP* **04**, 050 (2004).
19. R. Casalbuoni, G. Nardulli, *Rev. Mod. Phys.* **76**, 263 (2004).
20. M.G. Alford, A. Schmitt, K. Rajagopal, T. Schafer, *Rev. Mod. Phys.* **80**, 455 (2008).
21. R. Anglani, R. Casalbuoni, M. Ciminale, N. Ippolito, R. Gatto, M. Mannarelli, M. Ruggeri, *Rev. Mod. Phys.* **86**, 509 (2014).
22. M. Buballa, S. Carignano, *Prog. Part. Nucl. Phys.* **81**, 39 (2015).
23. H.G. Dosch, *Phys. Lett. B* **190**, 177 (1987); H.G. Dosch, Yu Simonov, *Phys. Lett. B* **205**, 339 (1988); Yu Simonov, *Nucl. Phys. B* **307**, 512 (1988).
24. A. Di Giacomo, H.G. Dosch, V.I. Shevchenko, Y.A. Simonov, *Phys. Rep.* **372**, 319 (2002).

25. Yu.A. Simonov, M.A. Trusov, *JETP Lett.* **85**, 598 (2007); Yu.A. Simonov, M.A. Trusov, *Phys. Lett. B* **650**, 36 (2007).
26. A.V. Nefediev, Yu.A. Simonov, A.M. Trusov, *Int. Jour. Mod. Phys. E* **18**, 549 (2009).
27. D. Blaschke, arXiv:1502.06279 (2015).
28. I. Bombaci, D. Logoteta, *Mont. Not. Royal Astr. Soc.* **433**, L79 (2013).
29. D. Logoteta, I. Bombaci *Phys. Rev. D* **88**, 063001 (2013).
30. G.F. Burgio, D. Zappalà, contribution to this Topical Issue.
31. Z. Berezhiani, I. Bombaci, A. Drago, F. Frontera, A. Lavagno, *Nucl. Phys. B - Proceedings Supplement* **113**, 268 (2002).
32. Z. Berezhiani, I. Bombaci, A. Drago, F. Frontera, A. Lavagno, *Astrophys. Jour.* **586**, 1250 (2003).
33. I. Bombaci, I. Parenti, I. Vidaña, *Astrophys. Jour.* **614**, 314 (2004).
34. I. Vidaña, I. Bombaci, I. Parenti, *Nucl. Phys. A* **754**, 345c (2005).
35. I. Vidaña, I. Bombaci, I. Parenti, *J. Phys. G: Nucl. Part. Phys.* **31**, S1165 (2005).
36. G. Lugones, I. Bombaci, *Phys. Rev. D* **72**, 065021 (2005).
37. I. Bombaci, G. Lugones, I. Vidaña, *Astron. and Astrophys.* **462**, 1017 (2007).
38. I. Bombaci, P.K. Panda, C. Providência, I. Vidaña, *Phys. Rev. D* **77**, 083002 (2008).
39. I. Bombaci, D. Logoteta, P.K. Panda, C. Providência, I. Vidaña, *Phys. Lett. B* **680**, 448 (2009).
40. I. Bombaci, *Int. Jour. Modern Phys. D* **19**, 1491 (2010).
41. I. Bombaci, D. Logoteta, C. Providência, I. Vidaña, *Astron. and Astrophys.* **528**, A71 (2011).
42. D. Logoteta, I. Bombaci, C. Providência, I. Vidaña, *Phys. Rev. D* **85**, 023003 (2012).
43. D. Logoteta, C. Providência, I. Vidaña, I. Bombaci, *Phys. Rev. C* **85**, 055807 (2012).
44. D. Logoteta, C. Providência, I. Vidaña, *Phys. Rev. C* **88**, 055802 (2013).
45. A. Drago, A. Lavagno, G. Pagliara, *Phys. Rev. D* **69**, 057505 (2004).
46. A. Drago, G. Pagliara, J. Schaffner-Bielich, *J. Phys. G* **35**, 014052 (2008).
47. C. Bambi, A. Drago, *Astropart. Phys.* **29**, 223 (2008).
48. A. Drago, A. Lavagno, I. Parenti, *Astrophys. Jour.* **659**, 1519 (2007).
49. B.W. Mintz, E.S. Fraga, G. Pagliara, J. Schaffner-Bielich, *Phys. Rev. D* **81**, 123012 (2010).
50. G. Lugones, A.G. Grunfeld, *Phys. Rev. D* **84**, 085003 (2011).
51. T.A.S. do Carmo, G. Lugones, A.G. Grunfeld, *Jour. Phys. G* **40**, 035201 (2013).
52. G. Lugones, contribution to this Topical Issue.
53. N.K. Glendenning, S.A. Moszkowski, *Phys. Rev. Lett.* **67**, 2414 (1991).
54. N.K. Glendenning, *Compact Stars: Nuclear Physics, Particle Physics, and General Relativity*, Springer, New York (2000).
55. E. Farhi, R.L. Jaffe, *Phys. Rev. D* **30**, 2379 (1984).
56. E. Fraga, R.D. Pisarki, J. Schaffner-Bielich, *Phys. Rev. D* **63**, 121702(R) (2001).
57. M. Alford, M. Braby, M. Paris, S. Reddy, *Astrophys. Jour.* **629** 969 (2005).
58. S. Weissenborn, I. Sagert, G. Pagliara, M. Hempel, J. Schaffner-Bielich, *Astrophys. Jour.* **740** L14 (2011).
59. P. Rehberg, S.P. Klevansky, J. Hufner, *Phys. Rev. C* **53**, 410 (1996).
60. H.J. Pirner, G. Chanfray, O. Nachtmann, *Phys. Lett. B* **147**, 249 (1984).
61. Drago A and Tambini E 1999 *J. Phys. G* **25** 971
62. I. Bombaci, B. Datta, *Astrophys. Jour.* **530**, L69 (2000.)
63. A.R. Bodmer, *Phys. Rev. D* **4**, 1601 (1971).
64. E. Witten, *Phys. Rev. D* **30**, 272 (1984).
65. C. Alcock, E. Farhi, A. Olinto, *Astrophys. Jour.* **310**, 261 (1986).
66. P. Haensel, J.L. Zdunik, R. Schaefer, *Astron. and Astrophys.* **160**, 121 (1986).
67. M. Dey, I. Bombaci, J. Dey, S. Ray, B.C. Samanta, *Phys. Lett. B* **438** 123 (1998); *Phys. Lett. B* **447** 352 (1999); *Phys. Lett. B* **467** 303 (1999).
68. X.-D. Li, I. Bombaci, M. Dey, J. Dey, E.P.J. van den Heuvel, *Phys. Rev. Lett.* **83**, 3776 (1999).
69. X.-D. Li, S. Ray, J. Dey, M. Dey, I. Bombaci, *Astrophys. Jour.* **527**, L51 (1999).
70. R. X. Xu, G. J. Qiao, and B. Zhang, *Astrophys. J.* **522**, L109 (1999).
71. M. Prakash, I. Bombaci, M. Prakash, P.J. Ellis, J.M. Lattimer, R. Knorren, *Phys. Rep.* **280**, 1 (1997).
72. G. Lugones, O.G. Benvenuto, *Phys. Rev. D* **58**, 083001 (1998).
73. G. Lugones, A.G. Grunferld, N.N. Scoccola, C. Villavicencio, *Phys. Rev. D* **80**, 045017 (2009).
74. I.M. Lifshitz, Y. Kagan, *Sov. Phys. JETP* **35**, 206 (1972).
75. K. Iida, K. Sato, *Phys. Rev. C* **58**, 2538 (1998).
76. H. Heiselberg, C.J. Pethick, E.F. Staubo, *Phys. Rev. Lett.* **70** 1355, (1993).
77. D.N. Voskresensky, M. Yasuhira, T. Tatsumi, *Nucl. Phys. A* **723**, 359 (2003).
78. G. Lugones, A.G. Grunferld, M Al Ajmi, *Phys. Rev. C* **88**, 045803 (2013).
79. J.R. Oppenheimer, G.M. Volkoff, *Phys. Rev.* **55**, 374 (1939).
80. I. Bombaci, S.B. Popov, *Astron. and Astrophys.* **424**, 627 (2004).
81. Z. Arzoumanian, D.F. Chernoff, J.M. Cordes, *Astrophys. Jour.* **568**, 289 (2002).
82. P. Demorest, T. Pennucci, S. Ransom, M. Roberts, and J. Hessels, *Nature (London)* **467**, 1081 (2010).
83. J. Antoniadis, et al. *Science* **340**, 1233232 (2013).
84. R.A. Hulse, J.H. Taylor, *Astrophys J.* **195**, L51 (1975); J.M. Weisberg, D.J. Nice, J.H. Taylor, *Astrophys J.* **722**, 1030 (2010).
85. A. Drago, A. Lavagno, G. Pagliara, D. Pigat, contribution to this Topical Issue.
86. A. Burrow, J.M. Lattimer, *Astrophys. Jour.* **307**, 178 (1986).
87. I. Bombaci, M. Prakash, M. Prakash, P.J. Ellis, J.M. Lattimer, G.E. Brown, *Nucl. Phys. A* **583**, C623 (1995).
88. J.A. Pons, S. Reddy, M. Prakash, J.M. Lattimer, J.A. Miralles, *Astrophys. Jour.* **513**, 780 (1999).
89. I. Vidaña, I. Bombaci, A. Polls, A. Ramos, *Astron. and Astrophys.* **399**, 687 (2003).
90. J. Margueron, I. Vidaña, I. Bombaci, *Phys. Rev. C* **68**, 055806 (2003).
91. I. Bombaci, *Astron. and Astrophys.* **305**, 871 (1996).

92. J.E. Horvath, O.G. Benvenuto, H. Vucetich, *Phys. Rev. D* **45**, 3865 (1992).
93. J. E. Horvath, *Phys. Rev. D* **49**, 5590 (1994).
94. M.L. Olesen, J. Madsen, *Phys. Rev. D* **49**, 2698 (1994).
95. T. Harko, K.S. Cheng, P.S. Tang, *Astrophys. Jour.* **608**, 945 (2004).
96. J.S. Langer, *Ann. Phys. (N.Y.)* **54**, 258 (1969).
97. J.S. Langer, L.A. Turski, *Phys. Rev. A* **8**, 3230 (1973).
98. L. Csernai, J.I. Kapusta, *Phys. Rev. D* **46**, 1379 (1992).
99. R. Venugopalan, A.P. Vischer, *Phys. Rev. E* **49**, 5849 (1994).
100. I. Sagert, T. Fischer, M. Hempel, G. Pagliara, J. Schaffner-Bielich, A. Mezzacappa, F.-K. Thieleman, M. Liebendörfer, *Phys. Rev. Lett.* **102**, 081101 (2009).
101. K. Nakazato, K. Sumiyoshi, S. Yamada, 2008, *Phys. Rev. D* **77**, 103006 (2008).
102. B. Dasgupta, T. Fischer, S. Horiuchi, M. Liebendörfer, A. Mirizzi, *Phys. Rev. D*, **81**, 103005 (2010).
103. S. Bhattacharyya, *Adv. Space Res.* **45**, 949 (2010).
104. A.W. Steiner, J.M. Lattimer, E.F. Brown, *Astrophys. Jour.* **722**, 33 (2010).
105. S. Bhattacharyya, A.V. Thampan, I. Bombaci, *Astr. and Astrophys.* **372**, 925 (2001).